CrossMark

ORIGINAL ARTICLE

Double-cusp simulation during northward IMF using 3D PIC global code

Amin Esmaeili[1] · Mohammad Javad Kalaee[1]

Abstract The cusp has important effects on the transportation of particles and their energy from the solar wind to the magnetosphere, and ionosphere, and high-altitude atmosphere. The cusp can be considered to be a part of the magnetospheric boundary layer with weaker magnetic fields. It has been studied since 1971 by different satellite observations. Despite many years of investigation, some problems, such as the boundaries, shapes, and method of construction, remain to be solved. The double cusp was first reported by Wing using the observation of the DMSP satellite. He also compared the results of observations with the results of a 2D MHD simulation. In this study, by performing simulations and analyzing the results, we report the observation of a V-shaped double-cusp structure under the northward Interplanetary Magnetic Field (IMF). In our simulation, the double cusp was seen only for electrons, although a weak double cusp was observed for ions as well. We showed that this double cusp occurred because of electron precipitation from different sources of solar wind and magnetosphere with different magnetic field strengths. In previous studies of the double cusp, there were debates on its spatial structure or on its temporal behavior due to the cusp movement caused by the sharp solar wind effects on the magnetosphere shape. Here we report the spatial detection of the double cusp similar to the one observed by the DMSP satellite, but for the northward IMF case. Also, we investigate the asymmetry along the dawn-dusk side of the magnetosphere using our 3D PIC simulation code.

✉ A. Esmaeili
amesmaeili@ut.ac.ir

M.J. Kalaee
mjkalaee@ut.ac.ir

[1] Institute of Geophysics, University of Tehran, Tehran, Iran

1 Introduction

The polar cusp was first observed by Heikkila and Winningham (1971) and Frank (1971). Since then, many studies including cusp's dynamics and particle precipitations have been done. The cusp is defined as a region of high density plasma, highly turbulent and depressed magnetic field, and stagnant flow (Zong et al. 2004; Cai et al. 2015). The double cusp includes two regions of high density and high energy at different latitudes of the cusp region, which originate from different latitudes of the magnetosheath area.

Wing et al. (2001) and Trattner et al. (2002) showed that the double cusp is a structure of a spatial nature. Figure 1 is an example of the double cusp observed by the DMSP satellite as reported by Wing et al. (2001). On April 18, 2002, a cusp-like region from 1620 to 1830 UT was observed three consecutive times by all four Cluster satellites (Zong et al. 2004). In all three observations, cusps were found to be related to the signatures of energetic ions. Zong et al. (2004) analyzed their results of the triple cusp in three ways—as temporal, spatial and hybrid temporal/spatial effects. In temporal effects, the first and second branches of the double cusp are the same cusp, moving due to the change in solar wind conditions in a short time, and so it was detected at a later time and different location. In spatial effects, both branches of the double cusp exist when the satellite reached them. In temporal/spatial effects, a combination of spatial and temporal features occurs: cusps 1 and 2 could be the double cusp (a spatial feature); the third cusp could be observed as a result of sharp change in IMF Bz/By that moves the high-altitude reconnection site (temporal effect). Finally, they concluded that the triple cusp could be a temporal ef-
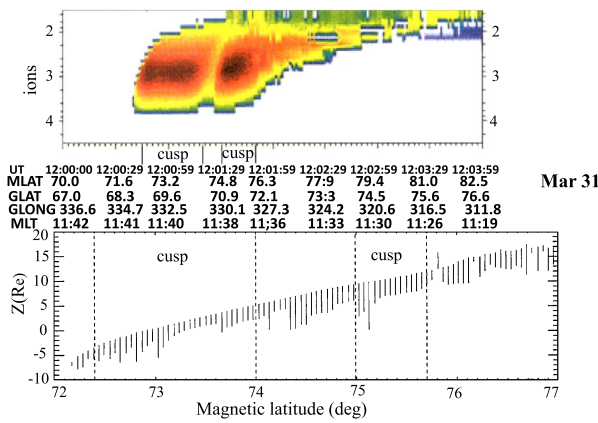
Fig. 1 (**a**) Double cusp observed by the DMSP satellite. (**b**) Double cusp, marked by dashed lines, observed at different latitudes. The plot is for the ion density, Wing et al. (2001)

fect, but the spatial effect or hybrid effect cannot be completely ruled out. In previous work, Escoubet et al. (2008) reported the double cusp as a special effect (07 Aug 2004 CLUSTER data). In the analysis of the other event (Escoubet et al. 2013), they reported that it could be a temporal effect (20 Aug 2002 CLUSTER data). As satellites may collect data under different conditions although they are at the same place, both of these theories seem to be correct. In this work we report the special double cusp for northward IMF case. We traced particles from about 400 time steps before formation of the double cusp to the 400 time steps after that formation. The double cusp was seen for electrons and was not detected for ions in the simulation results. We discuss double-cusp origins and the double-cusp asymmetry in the dawn-dusk sides of the meridian plane in Sects. 3.1 and 3.2, respectively.

2 Simulation model

We used the updated version of 3D Stanford PIC code (Tristan code) for our simulation (Buneman et al. 1992; Buneman 1993; Cai et al. 2015). The simulation model is a three-dimensional electromagnetic full particle global simulation model with the whole time sequence of the IMF rotations as follows: phase (i), from time step 0 to 1500; there is no IMF and the magnetosphere is generated using a magnetic dipole field; phase (ii), a northward IMF ($Bz = 0.215$) is gradually turned on from 1501 to 1800. After that, IMF has no changes until time step 3000.

The basic equations are as follows:

$$\frac{\partial \mathbf{B}}{\partial t} = -c\nabla \times \mathbf{E}, \tag{1}$$

$$\frac{\partial \mathbf{E}}{\partial t} = c^2\nabla \times \mathbf{B} - \frac{1}{\varepsilon_0}\mathbf{J}, \tag{2}$$

$$m_{i,e}\frac{d\mathbf{v}_{i,e}}{dt} = q_{i,e}(\mathbf{E} + \mathbf{v}_{i,e} \times \mathbf{B}), \tag{3}$$

where B, E, J, c are the magnetic, the electric field, electric current density and the speed of light, respectively. V, q, and m denote the velocity, charge of particle and mass of the particle, respectively; the subscripts e and i stand for electrons and ions.

We assume the grid spacing $\Delta x = \Delta y = \Delta z = \Delta$ to be $0.5R_e$, where R_e is the radius of the Earth, and the time step Δt to be $0.125\omega_{pe}^{-1}$, where ω_{pe} is the electron plasma frequency. The number of grids are assumed to be in x, y, and z directions, respectively. Initially, we use about 3.6×10^7 *electron–ion* pairs, which corresponds to a uniform particle density of $n_e = n_i = 8$ pairs for each cell across the simulation box. The normalized physical values ($\tilde{}$) are defined as follows. The thermal velocity is

$$\tilde{v}_{the,i} = v_{the,i}/(\Delta/\Delta t). \tag{4}$$

The Debye length is

$$\tilde{\lambda}_{De,i} = \tilde{v}_{the,i}/\tilde{\omega}_{pe,i}. \tag{5}$$

The inertia length is

$$\tilde{\lambda}_{ce,i} = \tilde{c}/\tilde{\omega}_{pe,i}, \tag{6}$$

where $\tilde{c}$ is the normalized speed of light. The Larmor gyroradius is

$$\tilde{\rho}_{ce,i} = \tilde{v}_{the,i}/\tilde{\omega}_{ce,i}. \tag{7}$$

The gyro frequency is

$$\tilde{\omega}_{ce,i} = \tilde{\omega}_{ce,i}\Delta t = eB\Delta t/m_e = \tilde{B}m_e/m_{e,i} \tag{8}$$

in which B is the magnetic field magnitude. The plasma beta is given by

$$\tilde{\beta} = (\tilde{T}_e + \tilde{T}_i)\tilde{\omega}_{pe}/\tilde{B}. \tag{9}$$

T is the particles' temperature. The values of the normalized ambient plasma parameters used in our simulation are $\tilde{v}_{the,i} = (0.09, 0.045)$; $\tilde{\lambda}_{De,i} = (0.75, 1.5)$; $\tilde{\lambda}_{Ce,i} = (4.2, 16.1)$; $\tilde{\omega}_{pe,i} = (0.125, 0.031)$; $\tilde{\omega}_{ce,i} = (0.45, 3.5)$; $\tilde{\beta}_{e,i} = (0.2, 0.8)$; and $\tilde{T}_{e,i} = (0.008, 0.032)$. Here, $\tilde{c} = 0.5$ is the normalized speed of light, which is considered according to the Courant condition. The center of the current loop that generates the dipolar terrestrial magnetic field is located at $(80\Delta, 72\Delta, 72\Delta)$. Within the time range $0 < t < 3000\Delta t$ we have a drift velocity $\tilde{v}_{solar} = 0.5\tilde{c}$, representing the solar wind continuously applied along the x-direction during the simulation within the time limit $0 < t < 3000$. The injected solar wind density also has $\tilde{n} = 8$, electron–ion pairs per cell and the mass ratio is $\frac{m_i}{m_e} = 16$; the electron and the ion thermal velocities are $\tilde{v}_{the,i} = (0.125, 0.625)$, respectively. All the real physical values can be obtained from the normalized parameters. The minimum distance from the Earth center to the dayside magnetopause R_{mp} is about 20 grid size

Table 1 Initial plasma conditions. β is plasma beta, B_{IMF} is the Interplanetary magnetic field and M_{Alfven} is the Mach Alfvén number

Grids	$215 \times 145 \times 145$
Initial particles	36000000 (8 pairs/cell) for each Electron and Ion
ε_0	1.000
m_i/m_e	16
q_e/m_e	0.500
dt/dx	$1.0/1.0 = 1.0$
Solarwind speed	0.200
Temperature	Ti = 0.032, Te = 0.008
$\omega_{pe}\,dt$	0.125
λ_e/dt	0.75
ρ_{cei}/dt	0.45 (electron), 3.5 (ion)
β	0.2
B_{IMF}	0.215
M_{Alfven}	0.98

Δ in our simulation. R_{mp} and the solar wind velocity scale all the physical values. For example if one assumes $R_{mp} = 64\,000$ km (i.e., $10R_E$ where $R_E = 6400$ km is the Earth radius) and the solar wind velocity $V_{SW} = 300$–600 km/s (here 400 km/s is a typical value), then the grid size Δ would be about 3400 km, 1000 time steps in the simulation would be about 7–14 min. The electron Debye length would be about 1792 km. All normalizations and parameters are summarized in Table 1.

In the current work, we discuss initial results of our global simulation, focusing mainly on the purely northward $(+|Bz|, 0, 0)$ case and on the high-altitude outer magnetospheric regions. We use the low regime of Alfvén Mach of 2.6 in the solar wind area.

3 Results and discussion

3.1 Double-cusp origins

We observed a v-shaped double cusp similar to the one reported in Escoubet et al. (2008). It is mainly for electrons for

the northward IMF direction at time step 2900 in the meridian plane as in Fig. 2(a). Also we have a weak double cusp observed for ions as shown in Fig. 2(b).

Particles were selected at the spheres, so that the numbered circles (Fig. 2) show the cross section of these spheres with the meridian plane. Circles numbered 1–12 in Fig. 2(a) show the places of 546 electrons sampled from the meridian plane along two branches of the double cusp. These include a group with five circles, 1–5, along the first branch and another group with circles numbered 6–10 along the second branch of the double cusp. Groups 11 and 12 are samples in the area between the branches of the double cusp. 178 electrons from groups 1–5, 228 electrons from groups 6–10 and 140 electrons from groups 11 and 12 were sampled. Nine circles shown in Fig. 2(b) are the places of 1081 sampled ions from the meridian plane along two areas of the double cusp. The first area had one circle and the second area eight circles; the first branch with circle number 1 is a weak part of the double cusp compared to the areas 2–8. The group 9 is sampled in the area between the branches of the double cusp for ions. 101 ions from group 1, 936 ions from groups 2–8 and 44 ions from group 9 are sampled.

The electron density profiles from time step 2400 to time step 2900 are shown in Fig. 3. It shows the formation of the double cusp from time step 2700 by penetration of magnetosheath electrons to the magnetosphere. Then magnetospheric electrons start to separate from the lower-altitude part of the cusp at time step 2800. Finally they separate in a V-shape at time step 2900. One possibility is that the part marked with an oval in the lower altitude of the cusp in time step 2800 is an addition of electrons already trapped in the magnetosphere. The 3D plot in Fig. 4(b) and particle trajectory in Fig. 6(a) could confirm this. This possibility matches our self-consistent tracing from 3D PIC simulation. Our tracing results in this subsection show that the double cusp originates from different sources rather than having the same origin.

The order of IMF rotation is such that the first dipole field of the magnetosphere will be built from the first step of the

Fig. 2 (a) Electron density profile during northward IMF direction at time step 2900 in the meridian plane. V-shaped double cusp is seen in the middle altitude of magnetosphere. Circles marked with numbers represent the spheres selected for tracing 12 groups of particles. (b) the same profile for ion density in the meridian plane. Circles marked with numbers represent the spheres selected for tracing 9 groups of ions
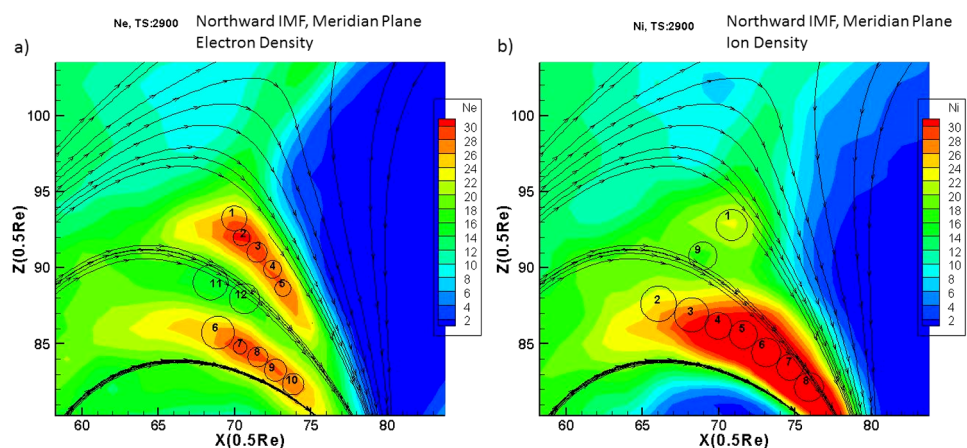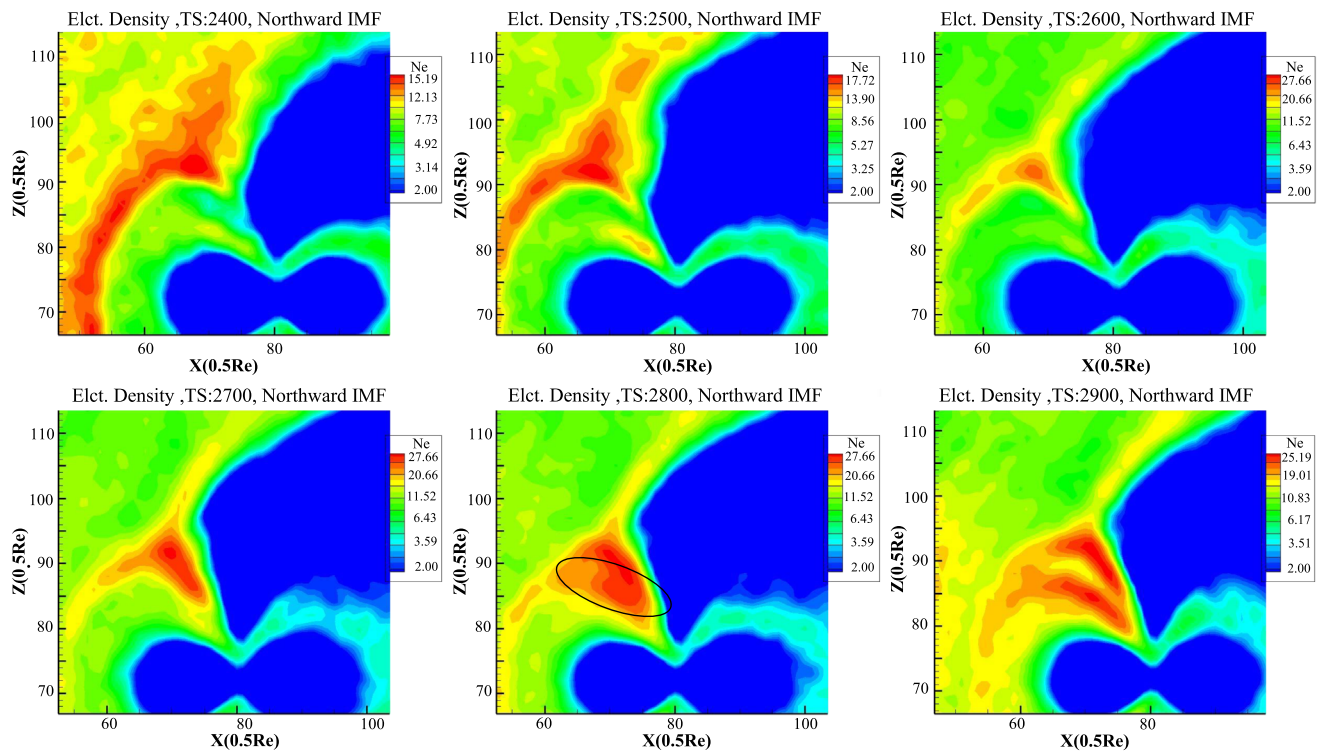
Fig. 3 Electron density profiles from time step 2400 to time step 2900 showing the double-cusp formation

Fig. 4 3D sample electron trajectories from 2600 time step to 3400 time step. Spheres show the place of electrons in every 20 time steps. (**a**) Sample electron trajectory passing from group 2 of double cusp in Fig. 2(a). (**b**) Sample electron trajectory passing from group 7 of double cusp in Fig. 2(a). The start of the path is in the left side of the simulation box and the ending is at the left side of the box. *Green lines* show the magnetic field streamlines during northward IMF case. (**c**) Sample ion trajectory passing from group 1 of double cusp in Fig. 2(b). (**b**) Sample ion trajectory passing from group 5 of double cusp in Fig. 2(b)
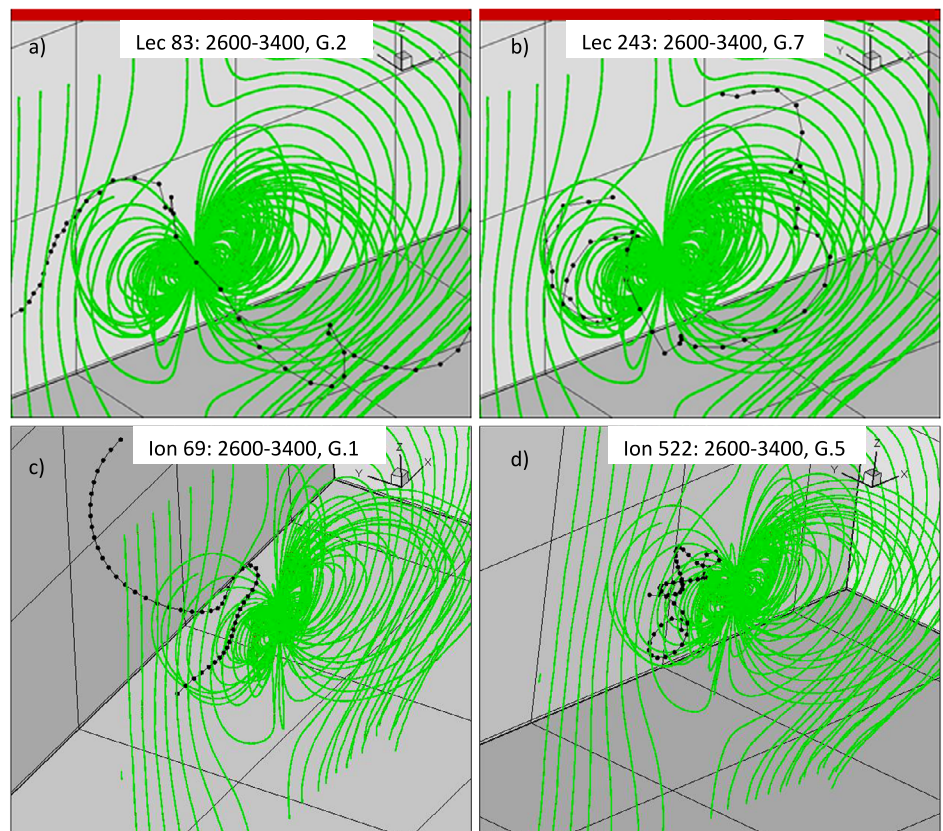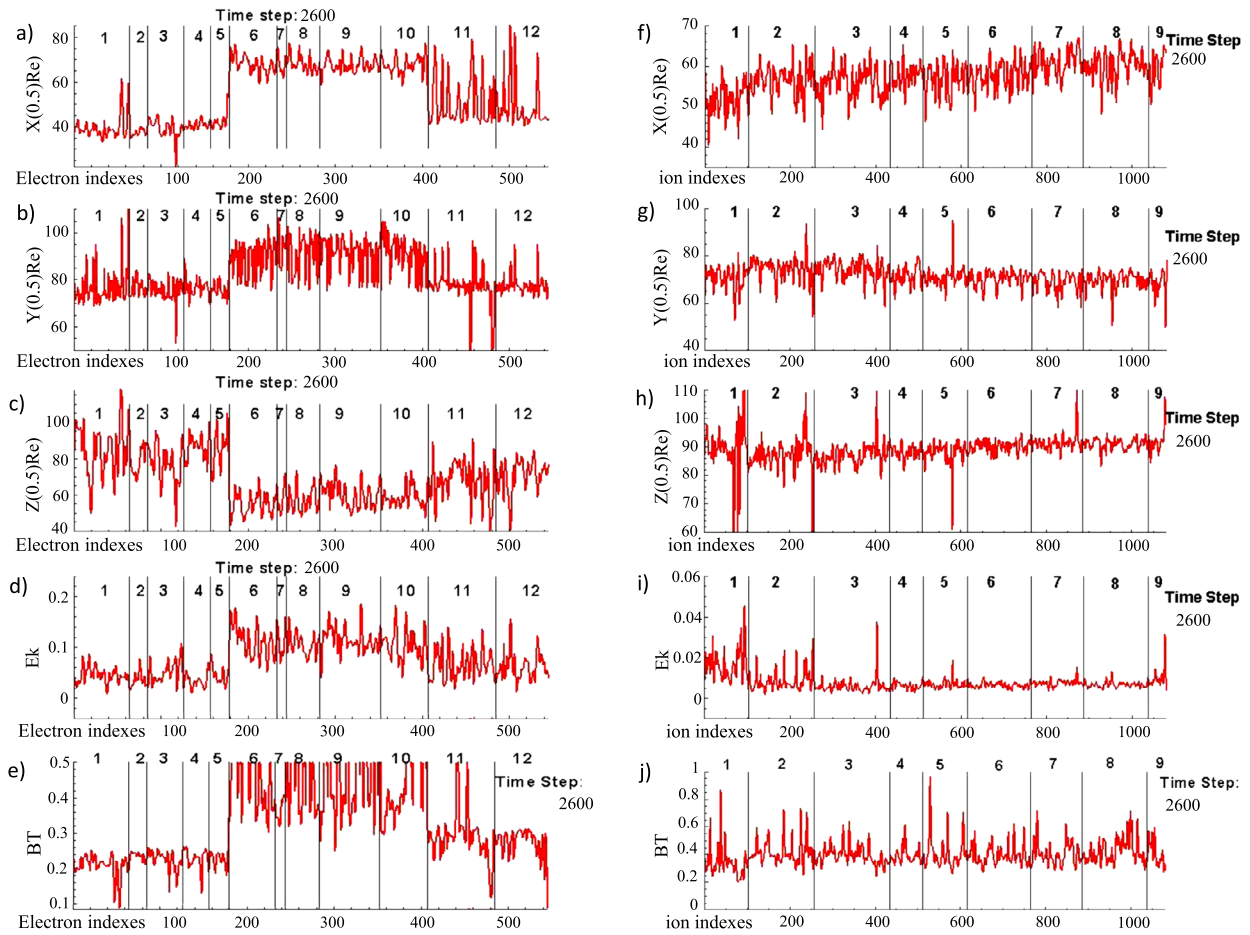
Fig. 5 (**a**)–(**c**) X, Y and Z position of 546 electrons at the start of the trajectory, time step 2600 (first point in the path of sample electron at the left side of simulation box in Fig. 2). The *vertical line* shows the electrons belonging to group 1 to group 12 of Fig. 2. (**d**) Energy of 546 electrons at the beginning of their trajectory, time steps 2600, 2900.

(**e**) Total magnetic field at the place of 546 electrons at the beginning of the trajectory. Vertical lines divide the 12 electron groups representing the double cusp and the area between them in Fig. 2. (**f**)–(**j**) is for the same plots for the 1081 ions in the nine groups corresponding to Fig. 2(b)

simulation. The simulation will continue in order to have a stable dipole magnetic field effective on the whole 3D box. Then the northward IMF will turn on at the left boundary of the box and remain fixed until time step 2900 so that the IMF spreads through the whole box.

In order to see how the double-cusp structure could be formed, we trace particles from about 400 time steps before to 400 time steps after the formation of the double cusp. Further, we sampled the data every 20 time steps. Figure 4(a), (b) shows the 3D trajectories of two sample electrons from group (2) and group (7) and Fig. 3(c), (d) shows the 3D trajectories of two sample ions from group (1) and group (5), respectively.

Green lines are the magnetic field streamlines from the simulation. In Fig. 4(a), a sample electron enters the upper branch of the double cusp from the solar wind. In Fig. 4(b), another sample particle, already trapped in the magnetosphere, enters the lower branch of the double cusp inside the magnetosphere.

In order to examine particles, we tried to investigate the particles locations, energies and the magnetic field strengths at the start of their trajectory at time step 2600. Figure 5(a)–(c) shows the X, Y and Z location of all 546 electrons at time step 2600, which is approximately the time at which particles in groups (1–5) (in Fig. 2(a)) start their journey from the left side of the box. Figure 5(d), (e) shows the total kinetic energy and magnetic field strength of 546 electrons at time step 2600. Figure 5(f)–(j) shows the same values for the 1081 ions.

As Fig. 5(a)–(c) shows, the electrons in both branches of the double cusp (groups 1–5, 6–10) originate from different parts of the simulation box. Electrons in groups (1–5) originate from the outside of the magnetosphere and electrons in groups (6–10) originate from the inside of the magnetosphere.

Figure 5(d) shows that electrons in the first branch of the double cusp (groups 1–5 in Fig. 2(a)) have lower energies than the electrons in the second branch (groups 6–10).

Fig. 6 Trajectories of two
particles each from different
groups of 1 and 2 in the
(**a**) Meridian (XZ),
(**b**) Equatorial (XY), (**c**) YZ
planes. These two particles are
different from those in Fig. 4(a),
(b). *Black traces* represent
particles in group 1 and the *blue
traces* show the path for the
electron in group 2. The *solid
line* shows the trajectory before
time step 2900 (double cusp).
Dashed lines shows the
trajectory after the double cusp
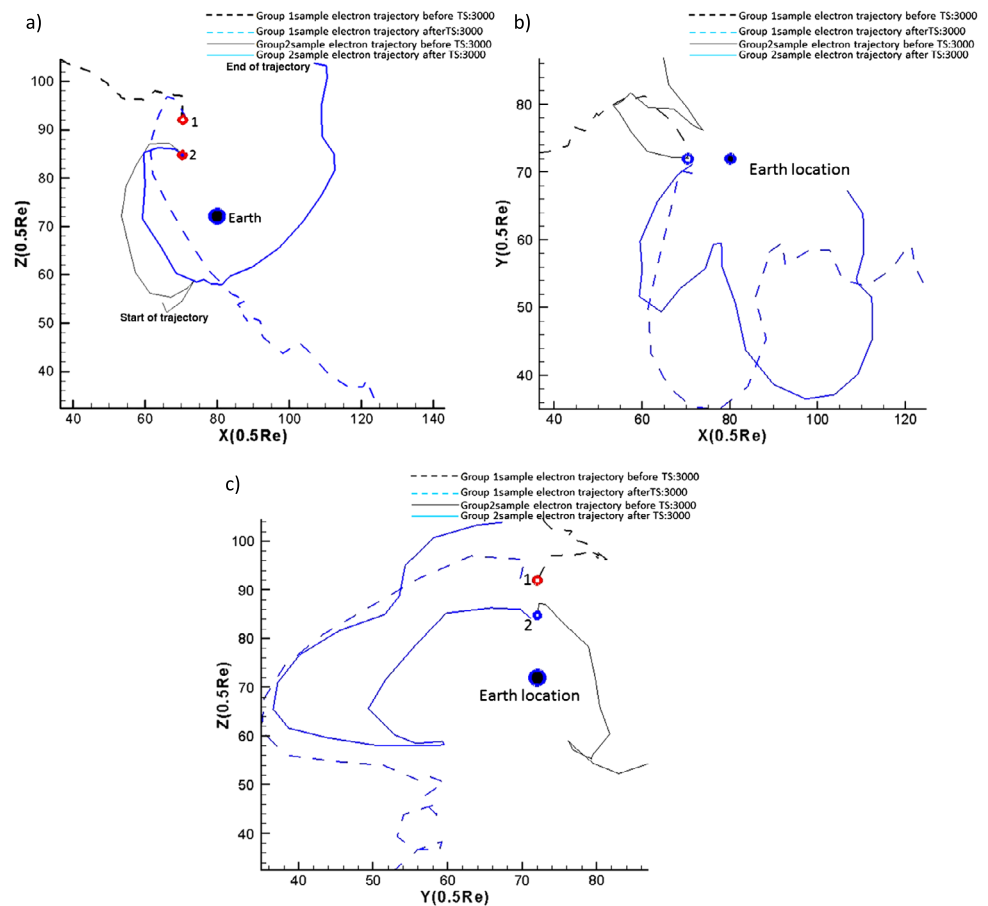
The electrons in the second branch are in lower altitude and come from the inside part of the magnetosphere. The higher energies of the particles trapped in the magnetosphere could be the result of different drifts, which they may undergo while in the magnetosphere. The energy graph supports the conclusion that particles with higher energies penetrate to the deeper areas of the magnetosphere. Figures 5(a)–(e) show that electrons in the groups 11 and 12, located between the two branches of double cusp (in Fig. 2(a)), originate from different areas from electrons in the double-cusp branches. Their origin is more similar to the higher-altitude branch of the double cusp. Further, their energies and magnetic field strength are similar to the electron energies in the first branch of double cusp (groups 1–5). For the ions in Fig. 5(f)–(j), we see that there is little difference between ions in group 1 and those in groups 2–8. There is only a slight difference in their location and their energies. The ions in group 1 are slightly more energetic than the ions in the groups 2–8.

Figure 6 shows the two sample electron trajectories in the meridian (XZ), equatorial (XY) and YZ planes. These two electrons are different from the particles traced back in Fig. 4(a), (b). The trajectory shown by the dashed line travels from the upper branch of the double cusp and the trajectory

shown by the solid line is from the lower branch. The black line represents the trajectory before time step 2900 and the blue line represents the trajectory after time step 2900.

It seems that the electron sampled in the upper branch of the double cusp entered the double cusp from the solar wind and the electron sampled in lower branch entered the lower-altitude branches of the double cusp from the magnetosphere. The electron belonging to the lower branch came from the solar wind as well, but it was trapped in the magnetosphere, probably in the outer Van Allen belts, and then entered the lower branch of the double cusp from there.

3.2 Double-cusp asymmetry in dawn-dusk side of the meridian plane

The cusp asymmetries in the dusk side and dawn side of the meridian plane are shown in Fig. 7(a) and (b).

Figure 7(a) shows that the electron density at the dusk side of the meridian plane at the time step equals 2900 for the northward MF case and Fig. 6(b) shows the electron density on the dawn side. As shown in Fig. 7(b), the cusp has the same v-shaped structure as in the meridian plane, but it is located at lower altitudes in comparison to the meridian plane. On the dusk side, the double cusp still exists but

Fig. 7 Electron density (**a**) at the dusk side ($y = 62$ (+5Re)) of the meridian plane at the time step: 2900 for the northward MF case, (**b**) at the dawn side of the meridian plane at the time step: 2900 for the northward MF case. Blacked arrow lines show the stream lines of magnetic field. Earth is located at (80, 72, 72)

a) Electron density, Y=62 (+5Re), TS: 2900

b) Electron density, Y=82 (-5Re), TS: 2900
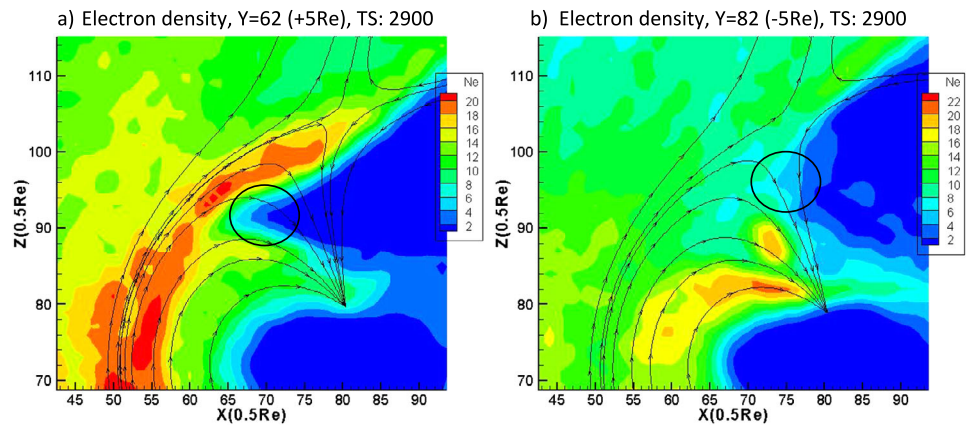
with separated radial structure on the boundary of the magnetosphere. Further, it is located at higher altitudes in comparison with the meridian plane. The circles in Fig. 7(a), (b) show the magnetosphere flanks. The penetration of the particles is apparently related to the different altitude of the magnetosphere. This could be one reason for the double-cusp structures in the dawn-dusk sides of the meridian plane being different.

4 Summary

In this simulation, we reported the double cusp by numerical simulation and tried to investigate the origins of the double cusp observed during the northward IMF case. A double cusp was observed for the electrons and a weak one was detected for the ions in the meridian plane. By tracing the electrons passing from the double cusp at time step 2900, we found that the higher branch of the double cusp was formed by electrons coming from the solar wind and the lower part was formed by electrons already trapped in the magnetosphere, probably in the outer Van Allen belts. Both cusps originate from the outside of the magnetosphere, as they come from the left side of the simulation box. However, particles forming the lower-altitude part may be delayed, energized by the magnetosphere and affected by different magnetospheric $\mathbf{E} \times \mathbf{B}$ drifts. The initial electron energies entering the lower branch of the double cusp were higher than the initial electron energies of the higher part of the double cusp. The more energy, the deeper electrons could penetrate into the cusp. We also traced ions forming a weak double cusp for the northward IMF case. We found there is only a minor difference between the ions entering the higher and lower altitudes of the double cusp. Further, we investigated the electron double-cusp asymmetry in the D–D sides of the magnetosphere. The results of this investigation indicated that the magnetosphere flanks on the dusk side of the mag-

netosphere prevent particles from entering the deeper parts of the cusp and forming the double cusp.

References

Buneman, O., Neubert, T., Nishikawa, K.I.: Solar wind-magnetosphere interaction as simulated by a 3-D EM particle code. IEEE Trans. Plasma Sci. **20**(6), 810–816 (1992)

Buneman, O.: TRISTAN: the 3-D, EM particle code. In: Matsumoto, e.b.H., Omura, Y. (eds.) Computer Space Plasma Physics, Simulation Techniques and Software, pp. 67–84. Terra Scientific, Tokyo (1993)

Cai, D., Esmaeili, A., Lembège, B., Nishikawa, K.-I.: Cusp dynamics under northward IMF using three-dimensional global particle-in-cell simulations. J. Geophys. Res. Space Phys. **120**, 8368–8386 (2015). doi:10.1002/2015JA021230

Escoubet, C.P., Berchem, J., Bosqued, J.M., Trattner, K.J., Taylor, M.G.G.T., Pitout, F., Laakso, H., Masson, A., Dunlop, M., Dandouras, I., Reme, H., Fazakerley, A.N., Daly, P.: Effect of a northward turning of the interplanetary magnetic field on cusp precipitation as observed by cluster. J. Geophys. Res. **113**, A07S13 (2008). doi:10.1029/2007JA012771

Escoubet, C.P., Berchem, J., Trattner, K.J., Pitout, F., Richard, R., Taylor, M.G.G.T., Soucek, J., Grison, B., Laakso, H., Masson, A., Dunlop, M., Dandouras, I., Reme, H., Fazakerley, A., Daly, P.: Double cusp encounter by cluster: double cusp or motion of discussions cusp? Ann. Geophys. **31**, 713–723 (2013). doi:10.5194/angeo-31-713-2013

Frank, L.A.: Plasma in the Earth's polar magnetosphere. J. Geophys. Res. **76**, 5202–5219 (1971)

Heikkila, W.J., Winningham, J.D.: Penetration of magnetosheath plasma to low altitudes through the dayside agnetospheric cusps. J. Geophys. Res. **76**, 883–891 (1971)

Trattner, K.J., Fuselier, S.A., Peterson, W.K., Carlson, C.W.: Spatial features observed in the cusp under steady solar wind conditions. J. Geophys. Res. **107**(A10), 1288 (2002). doi:10.1029/2001JA000262

Wing, S., Newell, P., Ruohoniemi, J.: Double cusp: model prediction and observational verification. J. Geophys. Res. **106**(A11), 25571–25594 (2001)

Zong, Q.-G., Fritz, T.A., Zhang, H., Korth, A., Daly, P.W., Dunlop, M.W., Glassmeier, K.-H., Reme, H., Balogh, A.: Triple cusps observed by cluster—temporal or spatial effect? Geophys. Res. Lett. **31**, L09810 (2004). doi:10.1029/2003GL01912